Swath Bathymetry and SAS Autofocus using a Chirp Source

Geoffrey Shippey[1] and Olle Kröling[2]

[1]Dept of Applied Electronics
Chalmers University of Technology
S-412 96 Gothenburg, Sweden
Email: gsh@ae.chalmers.se

[2]SubVision AB
Bredgatan 18
S-222 21 Lund, Sweden
Email: subvisab@algonet

Abstract

Swath bathymetry and SAS autofocus can both be treated as problems in correlating echoes from a scatterer distribution on the seabed. Using a chirp source, the phase derived from quadrature match-filtering can replace the narrowband phase in complex correlation operations. Pulse compression then enables bathymetry to be estimated more easily and accurately than with the corresponding narrowband processing. Using similar processing, the SAS auto-focus method gives direct estimates of unknown cross-track platform displacement. Field experimental equipment for the Swedish project is briefly described.

1. Introduction

The research presented here has been carried out under the Swedish DAIM (Digital Acoustic IMaging) Project. Emphasis is on high-frequency wideband insonification to maximise resolution at short range. Earlier papers [1,2] described the application of quadrature match-filtering to sidescan imaging and synthetic-aperture processing. The present paper concentrates on the inverse problem of swath bathymetry. SAS autofocus will also be addressed rather briefly since the two problems are more closely related than may appear at first sight. Swath bathymetry can be regarded as a problem in correlating echoes from a random distribution of reflectors on the seabed received at apertures separated in elevation. For synthetic-aperture auto-focus, the apertures are separated in the along-track direction.

2. State-of-the-Art

2.1 Sonar Imaging

Consider a linear array of receiver transducers with a plane echo wavefront arriving at azimuth angle θ from a reflector in the far field (Fig 1). Time-delay beamforming aligns the echoes from reflectors at angle θ by compensating for differential time-delays between the arrival of the wavefront at each transducer in turn. Because of its essential simplicity, there have been many attempts to find a digital implementation of time-delay beamforming. Superficially this appears easy, because echoes can be aligned in store by sample shifting. Unfortunately angular resolution is coarse unless the sampling frequency is high compared with the acoustic frequency, and this has led to a number of interpolation schemes over the years, eg [3,4].

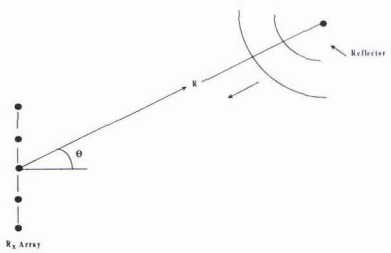

Fig 1. Sonar reception with a linear array

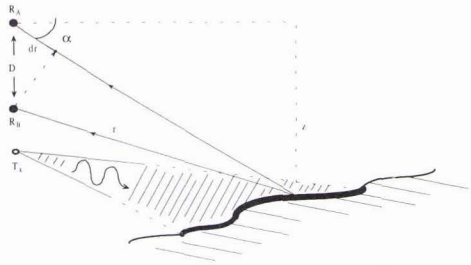

Fig 2. Bathymetric estimation : $z \approx r.dr / D$

2.2 Swath Bathymetry

Swath bathymetry is the operation of determining a depth map, or digital terrain model, from the elevation angle of echoes arriving from different slant ranges. For each output pulse or "ping", a profile of the seabed each side of the survey vessel can be computed, enabling the surface model to be built up as the sonar moves through the water. For shallow angles of incidence, an interferometric technique can be used [5]. Here elevation angle is inferred from the differential time-delay between the arrival of echoes at receivers spaced in elevation (Fig.2). This time difference is itself inferred from the differential phase of the echoes. [5] describes an elegant method in which analog echoes received at R_A and R_B are I and Q sampled to give complex echo sequences $\{a(n)\},\{b(n)\}$. The differential phase $\Delta\phi(r)$ in the neighbourhood of $n=r$ is given by the phase angle of the local ccf with zero displacement:

$$\gamma(r,r) = \sum_{k=-½L}^{L} w(l)\, a(r+k)\, b^*(r+k) \qquad (1)$$

where $w(l)$ is some taper function of length L, eg a Hanning window function. With narrowband echoes this local differential phase is still extremely noisy, even when L is large, so considerable smoothing is required. The consequent depth error depends on the baseline D. If this exceeds ½λ, the phase angle given by (1) is ambiguous. This ambiguity must be resolved by phase unwrapping, although problems can arise where there are step discontinuities in the scattering surface. To avoid such problems, "multibeam" systems such as the SIMRAD EM1000 [6] have been developed. Here a number of physical split-apertures are mounted around the hull of the survey vessel, and a large number of distinct elevation beams are constructed by a combination of aperture selection and beam-steering. Phase is now only used to determine the cross-over point of the beams from each split aperture.

2.3 "Auto-Focus" with Synthetic Aperture Sonar

Synthetic aperture sonar (SAS) is the acoustic analogue of SAR (synthetic-aperture-radar), routinely used to generate radar maps of the earth's surface. SAS would seem to be simpler to implement than SAR because of the lower frequencies involved. Unfortunately there are special problems with the water medium. Firstly the propagation time to the target and back varies from ping to ping unless the water is very calm. Movement of the sonar platform through the water is also subject to perturbation, leading to uncertainty in the relative positions of the sonar platform along the aperture. In side-looking mode, the lateral position of the sonar platform should be known within a fraction of the acoustic wavelength, ie to 1mm at cm acoustic wavelengths. Such accuracy is impossible to achieve by dead reckoning unless an expensive inertial platform is used, so reported experiments have been carried out at relatively low acoustic frequencies [7,8]. For airborne SAR, deviations of the platform track from a straight line have led to the development of auto-focus techniques where platform position is corrected from the image itself. The term "auto-focus" arises from methods where the platform track is perturbed until the best focus is obtained in the resulting SAR image [9]. For sonar, more direct methods have recently been proposed. Johnson, Hayes and Gough [10] describe a method of inferring lateral platform movement by cross-correlation of side-scan echoes. The final correlation operation uses a similar expression to (1).

3. Quadrature Match-filtering and Precise Range Estimation

3.1 Quadrature Phase and Time Delays

If the seabed echo is treated as the convolution of the source pulse with a random distribution of surface reflectors, many properties of an algorithm can be derived by considering the idealised echo from an isolated reflector. Consider range estimation using a chirp pulse such as $f(u)$, (Fig.3) with a symmetrical envelope function. Time zero at $u=0$ lies in the centre of the envelope. For digital processing, the received echo is sampled at regular time intervals τ_s. For match-filtering, the transmitted pulse is sampled to give $f_n = f(n\tau_s)$. The illustrated pulse has 129 samples, and a normalised frequency (with respect to sampling frequency) rising from 0.2 to 0.4 during the pulse length. Apart from a scale factor, the echo of $f(u)$ is $f(u\text{-}t)$ where t is the echo time. (pulse length = 2R+1 samples) for the required values of n. The analytic signal corresponding to the sampled pulse The sampled, delayed, echo $f(n\tau_s - t)$ will be denoted $f_n(t)$. Then the in-phase match-filtered echo is given by

$$p_n(t) = \sum_{|r|<R} f_r f_{n+r}(t) \qquad (2)$$

is given by

$$h_n = f_n + ig_n \qquad (3)$$

where $\{g_n\}$ is the Hilbert Transform of $\{f_n\}$. The quadrature match-filtered echo $z_n(t)$ is then expressed as

$$z_n(t) = p_n(t) + iq_n(t) = \sum_r h_r f_{n+r}(t) \tag{4}$$

The sequence of complex samples $\{z_n(t)\}$ has amplitude

$$e_n(t) = |z_n(t)| \tag{5}$$

and phase (which will be termed "quadrature phase"):

$$\phi_n(t) = arctan\text{-}((q_n(t)/p_n(t)). \tag{6}$$

Write t in the form $$t = N\tau_s + \tau, \quad |\tau| < \tfrac{1}{2}\tau_s \tag{7}$$

If t is an integral multiple of τ_s, e_n peaks at $n=N$ with $\phi_N = 0$. Otherwise e_n peaks at $n=N$ with non-zero phase. Appendix A shows that, subject to certain condition on the source signature, quadrature phase is the same linear function of t as analog phase for a carrier at the mid-frequency f_{mid}. The restrictions on the chirp pulse are

(i) carrier frequency should be a linear function of time (linear swept frequency chirp)

(ii) the pulse envelope should be symmetric about f_{mid}

(iii) this envelope should change slowly compared with the lowest chirp frequency present in the pulse.

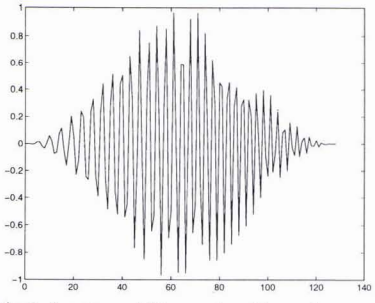

Fig 3. 1-octave, 128 sample, chirp pulse 0.2-0.4 normalised frequency

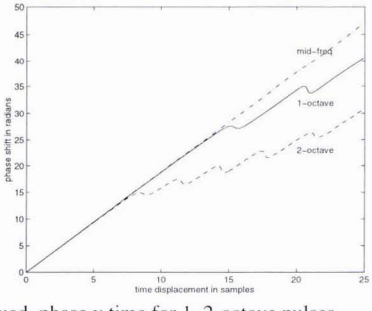

Fig 4. Quad. phase v time for 1, 2-octave pulses, analog phase for mid-frequency signal

Fig. 4 shows quadrature phase versus time displacement τ for a 1-octave and 2-octave chirp pulse. Phase-unwrapping is used to extend the phase-shift beyond $\pm\pi$. $\psi(x) = 2\pi f\tau$ is plotted for comparison, where f is the mid-frequency of the chirp pulses. The linear approximation remains good until the compressed envelope becomes small.

3.2 Polar Beamsteering

This digression on imaging will be helpful later on. Suppose we have a linear array of receiver elements R_k. It is required to point the receiver beam in a direction α with respect to the array normal. Then using the far-field approximation, time-delay beamsteering requires echoes from receiver transducer R_k at distance d_k from the array centre to be delayed with respect to echoes from the centre element by

$$t_k = (d_k/V)\ sin\ \alpha \tag{8}$$

For simplicity, the time delay t_k could be approximated by the nearest integer number of samples, m_k, and the k'th echo shifted by m_k samples in store. The receiver beam is then generated by taking the weighted sum over all transducers to generate the receiver beam. What is the angular resolution obtainable in this way? If $\frac{1}{2}\lambda$ spacing is used, the required time delay between adjacent echoes is given by

$$\Delta t \approx \alpha/2f \tag{9}$$

At a sampling frequency of f_s, the smallest time delay increment is $1/f_s$, so angular resolution is of order f/f_s. Beamsteering to 1° requires a minimum sampling frequency of $60\ f_{mid}$ unless some form of interpolation is used. By far the simplest interpolation method is to reverse the usual order of beamforming and rectification, and begin by quadrature match

filtering all transducer echoes. Each required time delay t_k is broken down into an integer number of sample intervals τ_s and a residue:

$$t_k = m_k \tau_s + \tau_k , \qquad | \tau_k | < \tfrac{1}{2} \tau_s \tag{10}$$

All the match-filtered samples from R_k are now shifted by m_k samples and phase-shifted by $\theta_k = 2\pi f_{mid} \tau_k$. The weighted sum of such shifted sequences over all the transducers gives a quadrature match-filtered receiver beam pointing in the direction α, and with the same sample spacing as the original transducer echoes.

3.3 Differential Range Estimation for Bathymetry using a Chirp Source.

Using a chirp source it is not possible to use expression (1) directly, since there is no longer a unique phase obtainable from I,Q filtering. One solution is to correlate the in-phase match filtered sampled echoes [12], but angular resolution is poor unless the sampling frequency is much higher than the acoustic frequencies. Instead it is to better to correlate the quadrature match-filtered echoes, which are complex valued so can be inserted directly into (1). After pulse compression, $|(m,n)|$ now has a well-defined peak for each m at $n = peak(m)$. Then

$$tdiff_m = [m - peak(m)]t_s \tag{11}$$

gives the best estimate of time displacement between echoes to the nearest integer number of sample intervals. The subsample time displacement is obtained from the phase, ϕ_m ,of

$$\gamma(m, peak(m)) = \sum_{k=-\frac{1}{2}L}^{\frac{1}{2}L} w(l)\, a(m+k)\, b^*(peak(m)+k) \tag{12}$$

The total time displacement is then given by

$$\Delta t = tdiff_m + \phi_m / 2\pi f_{mid} \tag{13}$$

For swath bathymetry, time difference is converted to differential range, and thence to elevation angle in the usual way. Since pulse compression enables a well-defined peak to be found in the ccf, there is no need to limit D to $\frac{1}{2}\lambda$ to avoid phase ambiguity. Much longer baselines can be used for elevation angle conversion.

4. Bathymetry Simulation

4.1 Simulation Model

The seabed was be modelled as a random distribution of surface scatterers. This is a plausible model for bathymetry at higher acoustic frequencies. Most properties of the bathymetric algorithm can be investigated using a simple one-dimensional model. The seabed profile was modelled as a random distribution of N scatterers/m with random reflectivity. N was varied from 100 up to 10000 reflectors/m. The scatterer distribution was also distributed randomly across the mean line of the slope in order to represent surface roughness. This distribution also accounts for the finite azimuth beamwidth, since variation between different profiles within the beamwidth contribute to the width of the vertical distribution. Two simple geometrical profiles were tested – HILL and STEPS (Figs.5a, b) – at horizontal ranges of 50 m. Sonar shadow was not modelled, so the back slope of HILL is not occluded by the front slope. Tests with STEPS established that the algorithm could cope with rapid changes in depth.

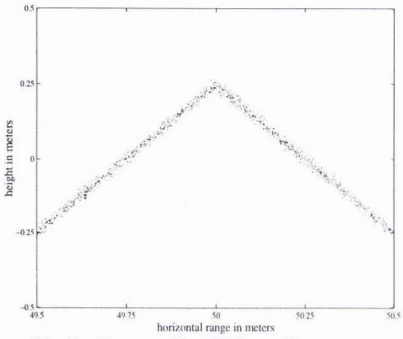

Fig 5a. Test profile HILL at 50 m range
500 reflectors/m, 1 cm lateral noise

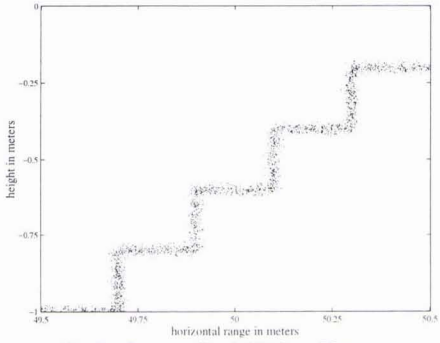

Fig 5b. Test profile STEPS at 50 m range
500 reflectors/m, 1 cm lateral noise

The acoustic mid-frequency was set at 150 kHz, giving a mid-wavelength λ_{mid} = 1 cm at a sound speed of 1500 m/sec. Sampling frequency was 500 kHz, giving a normalised mid-frequency f_{mid} = 0.3. With these parameters the 1-way differential distance corresponding to 1 sample interval is 3 mm. The 1 ms chirp pulse consisted of 512 samples with a Hanning envelope and a selectable bandwidth f_b. The value f_b=0.2 gives a 1 octave chirp pulse between 100 kHz and 200 kHz. Range resolution = $V/2f_b$ = 7.5 mm or 5 samples at the 100 kHz bandwidth. The vertical separation of the two receiver transducers was varied between $0.1\lambda_{mid}$ and 500 λ_{mid} , ie 1mm and 5m, with the transmitter located midway between them. White Gaussian noise could be added to the echoes. The length L of the correlation window was varied between 3 and 257, the latter corresponding to spatial smoothing of nominally 257 x 1.5 mm = 38 cm.

4.2 Simulation Results

Preliminary simulation runs were carried out in order to establish the qualitative effects of different parameters. Figs.6a,b show bathymetric estimates of HILL with N = 500 reflectors/m and 1 cm rms vertical noise. The processing parameters were 30 dB signal/noise ratio, 20 cm receiver separation, and a 17 sample window. These results demonstrate degraded profile tracking at lower bandwidths (strictly it is the absolute bandwidth which matters). Fig.7 shows a bathymetric estimate of STEPS with the same parameters, and a normalised bandwidth of 0.3.

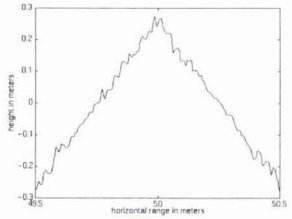

Fig 6a. Estimation of HILL,
normalised bandwidth = 0.4

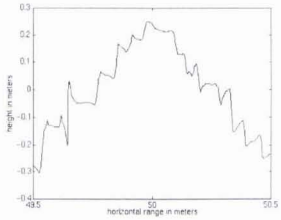

Fig 6b. Estimation of HILL,
normalised bandwidth = 0.05

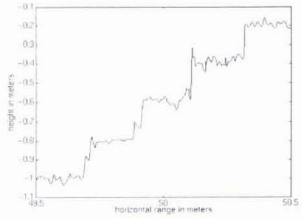

Fig 7. Estimation of STEPS,
normalised bandwidth = 0.3

Bathymetric accuracy was estimated by carrying out sets of 10 bathymetric runs, with different random reflector distributions and additive noise in each run. The error measure was the rms vertical difference in cms. between the bathymetric estimate and the profile centreline. Most results simply confirmed intuitive expectations, for example that performance deteriorates when a low reflector density, N, is combined with high profile noise, particularly if the window length is very short.. Rms errors of a few cms were obtained under most conditions, fairly independent of N.

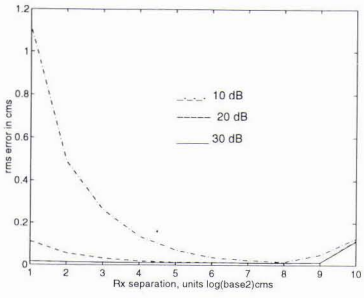

Fig 8a. Rms error versus receiver separation for SNR = 10, 20, 30 dB and bw = 0.3

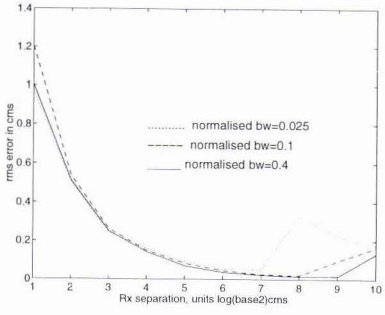

Fig 8b. Rms error versus receiver separation for bw = 0.025, 0.1, 0.4 and SNR = 10 dB

The more interesting results concern parameters which are under the system designer's control - correlation length, transducer separation, bandwidth. One question of particular interest concerns the choice of receiver separation. Fig.8a shows the effect of increasing receiver separation from 1 cm to 512 cm ($1\lambda_{mid}$ to 512 λ_{mid}) in the presence of noise. Around 50 cm separation gives best performance. When signal/noise ratio is high, the increase in receiver separation has a negligible effect on accuracy, implying no significant error other than that due to spatial resolution. For lower signal/noise ratios, accuracy improves with transducer separation, kappa, up to a certain limit. Fig.8b shows the effect of varying both separation and bandwidth, while keeping SNR fixed at 10 dB. This confirms that the useful region of kappa increases with bandwidth. For very large separations, accuracy falls off again due to misalignment between correlation windows for the upper and lower receiver apertures (Fig 9). When these are too far apart, the sample intervals resolved along the slope differ significantly in length, so samples can never be aligned along the whole length of the window.

4.3 Bathymetry Combined with Beam Steering

The proposed method of bathymetric processing can readily be combined with polar beamsteering (Fig.10). The simplest configuration is one where the transmitter beam provides the required azimuth resolution, while a split aperture with long axis in elevation is used for reception. Polar beamsteering is used to generate "multibeams" spanning the elevation angles of interest. The quadrature match-filtered sampled echo for each aperture generated by the polar beamsteering algorithm can be substituted directly into the bathymetric computation.

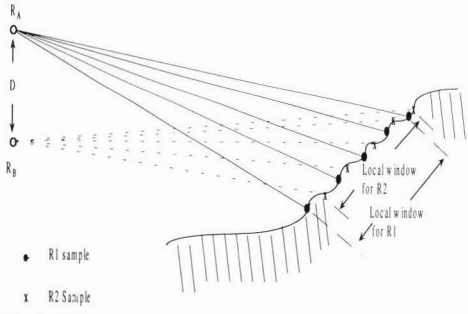

Fig 9. Misalignment of correlation windows

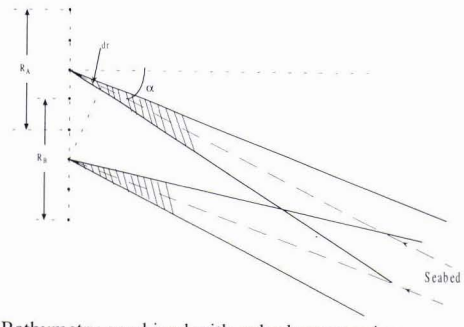

Fig 10. Bathymetry combined with polar beamsteering

5. Synthetic Aperture Auto-Focus

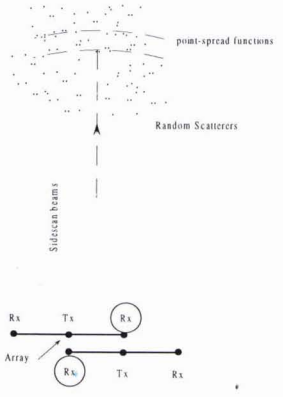

Fig 11. Compare echo from leading Rx, trailing array with trailing Rx, leading array

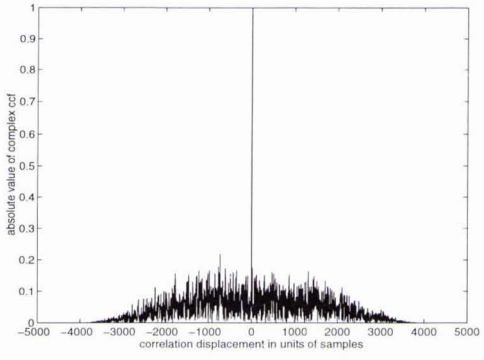

Fig 12. Echo ccf, 15 dB signal/noise ratio 500 random reflectors/m^2

5.1 Methodology

Johnson, Hayes and Gough [10] proposed the estimation of lateral platform movement by cross-correlation of sampled side-scan echoes. The author has investigated a similar method with the differences that quadrature match-filtered echoes are correlated, and that displacement is estimated both from the ccf peak position and the quadrature phase at the peak. Simulation studies show that lateral platform displacement can be estimated with high accuracy for small along-track displacements of the platform. However correlation fails completely when the along-track movement between pings approaches half the length of the receiver array – precisely the movement required for SAS processing [13]. A simple heuristic argument explains this phenomenon. Consider the point-spread functions for a particular echo sample in adjacent platform positions. For synthetic-aperture operation, the point spread function for the combined aperture, with platform positions half the receiver array length apart, is half the area of the separate psf's. Now suppose that the random reflectors in this combined footprint make a contribution to the echo of $\{z_i\}$. Then contributions for the individual footprints must be of the form $\{z_i\} \pm \{z_j\}$, where $\{z_j\}$ represents the contribution from random reflectors which are not in the combined footprint. The expected correlation between corresponding samples from adjacent positions is given by

$$\gamma = E\{\sum_i \sum_j (z_i + z_j)(z_i^* - z_j^*)\} = E\{\sum_i \sum_j (z_i z_i^* + z_j z_i^* - z_i z_j^* - z_j z_j^*)\} \qquad (14)$$

The expected contribution from the middle terms is zero, because of the random phases of the z_i and the z_j. The expected contribution from $z_j z_j^*$ cancels the contribution from $z_i z_i^*$, since the areas containing the two sets of reflectors are equal. Hence the expectation of γ reduces to zero as platform separation approaches half the length of the receiver array, and cross-correlation provides no information. Because of this problem, the alternative geometry of Fig.11 is proposed in order to align the point-spread functions for adjacent platform positions. The transmitter is located in the centre of the receiver array, and only the receivers at each end of the array are used for auto-focus. The platform moves precisely half this receiver array length between pings (pulses). For cross-correlation, the point-spread functions are aligned by comparing echo received by the leading transducer from the trailing array position with the echo received by the trailing transducer in the leading array position.

5.2 Simulation Studies

Simulation studies have been carried out with similar pulse parameters to Section 5, and a receiver array length of 1 m. The scatterers were distributed randomly over a 10 m x 10 m region. For simulation runs with 500 points/m^2 and 10 dB signal/noise ratio, the average error in estimating platform displacement was 60 μ. A typical ccf is shown in Fig.12. Correlation failed when SNR was reduced to 0 dB, though it succeeded again for sparser scatterer distributions. Using the

above method, it would be possible to align all platform positions in the synthetic aperture by successively aligning adjacent platform positions. However this is almost certainly not the optimum method of aligning a sequence of platform positions, since information available from other transducers on the platform is ignored. This optimization is planned as a main area for investigation, possibly as suggested in [11]. The sensitivity of correlation to scatterer density in the presence of noise is a matter for concern. The maximum density of 500 points/m^2 used in the simulation runs is not particularly high for sediment, since it corresponds to a scatterer spacing of several centimetres. On the other hand, a uniform random scatterer distribution is not representative of higher frequency sonar data, where some feature can usually be detected by eye, so there should be more information in real sonar echoes.

6. Experiments and Experimental Equipment

An experimental 32-channel sonar recorder has been designed by the Dept. of Technical Geology at Lund Technical University, in collaboration with SubVision AB who constructed the equipment. The recorder is designed for operation over a very wide bandwidth, 50-500 kHz, with sampling rates up to 2 MHz for each channel. Each channel includes a DSP chip to control sampling and other channel operations, as well as an individual hard disc. In future this DSP chip could be used for quadrature match filtering of all input echoes, required for both imaging and bathymetry. The large number of parallel channels allows a reasonably long array length for physical aperture imaging. It is also valuable for SAS processing, since the movement of the receiver array between pings is set by the length of the receiver aperture [1]. The technical objective is to combine good quality physical aperture images obtained at medium frequency into SAS images. This requires auto-focus techniques which perform well at centimetre wavelengths. The 32-channels can be split into separate apertures for bathymetry. Tank experiments have now begun, and the first experimental images obtained. The next stage is to move out to Malmö harbour for bathymetric and auto-focus experiments using real sea-bed. It is then planned to carry out lake experiments from a moving vessel in conjunction with Bofors Underwater Systems.

7. Conclusions

The paper has presented theoretical and simulation studies which imply radically superior performance for bathymetric sonar using a chirp source. If these studies are validated by field experiment, it could provoke a revival of interest in the simpler interferometric geometries, and further increase interest in chirp sonar developments. Interesting simulation results have also been obtained for SAS auto-focus, although here there is much theoretical work still to be done. However a powerful tool should be available for estimating cross-track positioning errors over "featureless" terrain. It is urgent to obtain experimental support for these claims, but also to obtain a more realistic seabed simulation model suitable for echo correlation investigations

8. Acknowledgments

The research presented was carried out with the support of the Swedish State Research Board, NUTEK, under the Autonomous Robotic Systems Programme. Technical support and advice from other partners in the Project – Peter Ulriksen at Lund Technical University, Klas Themner at Bofors Underwater Systems - is gratefully acknowledged.

9. References

[1] G.A. Shippey and T. Nordqvist, "Phase-array acoustic imaging in ground coordinates, with extension to synthetic aperture processing", *IEE Proc. Radar, Sonar, and Navigation*, vol. 143, pp. 131-139, June 1996.

[2] G.A. Shippey, "Simple Algorithms for sonar imaging and swath bathymetry using a linear-swept-frequency (chirp) source", *Proc. Int Conf. on Imaging and Image Interpretation*, Santa Barbara, Dec. 1996 (in press)

[3] R.G. Pridham and R.A. Mucci, "Digital interpolation beamforming for low-pass and band-pass signals", *Proc. IEEE*, vol. 67, pp 904-919, 1979.

[4] S. Ries, "Digital time-delay beamforming with interpolated signals", *Proc. European Conf. on Underwater Acoustics* (ECUA Luxembourg 1992), ed. M.Weydert , Elsevier, ECUA (Luxembourg) , pp.594-689

[5] M.A. Masnadi-Shirazi, C. de Moustier, P. Cervenka and S.H. Zisk: "Differential phase estimation with the SEAMARC II bathymetric sidescan sonar system", *IEEE J.Oceanic Eng.*, vol. 16, pp 239-250, July 1992.

[6] E. Hammerstad and F. Pohner, "Ultra wide swath deep sea interferometric multibeam echo sounder with sea bottom imaging system", *Proc.IEEE Oceans 90 Conf.* ,Washington, pp.63-68, 1990

[7] D.W. Hawkins and P.T. Gough, "Recent sea trials of a synthetic aperture sonar", *Proc. Inst. Acoustics* , vol. 17, Pt 8, pp. 1-10, 1995.

[8] M.A. Lawlor, V.S. Rayait, A.E. Adams, O.R. Hinton, and B.S. Sharif, "Results from sea-trals of a real-time synthetic processing system", *Proc. 3rd European Conference on Underwater Acoustics*, Ed J.S.Papadakis, Pub. FORTH-IACM, Heraklion, Crete, pp. 889-894, June 1996.

[9] D. Blacknell and S. Quegan, "SAR motion compensation using auto-focus", *Int. J. Remote Sensing*, vol. 12, no. 2, pp. 253-275, 1991.

[10] K.A. Johnson, M.P. Hayes, and P.T. Gough, "A method of estimating the sub-wavelength sway of a sonar towfish", *IEEE J. Oceanic Eng.*, vol. 20, no. 4, pp. 258-267, 1995.

[11] J. Chatillon and M.E. Zakharia, "Self-focusing of a synthetic aperture sonar in the case of bottom reverberation", *Proc. 3rd European Conference on Underwater Acoustic*, Ed J.S.Papadakis, Pub. FORTH-IACM, Heraklion, Crete, pp. 433-438, June 1996.

[12] J. Chatillon and M.E. Zakharia, "Validation of bathymetry algorithms using wideband synthetic aperture techniques by means of tank experiments", *Proc. 3rd European Conference on Underwater Acoustics*, Ed J.S.Papadakis, Pub. FORTH-IACM, Heraklion, Crete, pp. 427-43, June 1996.

[13] K.D. Rolt and H. Schmidt, "Azimuthal ambiguities in synthetic aperture sonar and synthetic aperture radar imagery", *IEEE J. Oceanic Eng.*, vol. OE-17, pp 73-79, Jan.1992.

10. Appendix A: Instantaneous Phase Measurement by Quadrature Match Filtering

Consider the chirp source signal $p(t) = A(t)\cos(ft + gt^2)$ (A1)

where A(t) is a symmetrical envelope function centred on t=0. If $A(t)$ varies slowly in comparison with the lowest period of the chirp, then the Hilbert Transform of $p(t)$,

$$q(t) \quad A(t)\sin(ft + gt^2) \tag{A2}$$

The in-phase match filtered signal is given by

$$P(\tau) = \int A(t-\tfrac{1}{2}\tau)A(t+\tfrac{1}{2}\tau)\cos[f(t-\tfrac{1}{2}\tau)+g(t-\tfrac{1}{2}\tau)^2]\cos[f(t+\tfrac{1}{2}\tau)+g(t+\tfrac{1}{2}\tau)^2]dt \tag{A3}$$

using symmetrical displacements for convenience. Then by standard trigonometry,

$$P(\tau) = P_1(\tau) + P_2(\tau)\ (\tau) = \tfrac{1}{2}\int A(t-\tfrac{1}{2}\tau)A(t+\tfrac{1}{2}\tau)\cos(f\tau + 2gt\tau)dt \tag{A4}$$

where $P_2(t) = \tfrac{1}{2}\int A(t-\tfrac{1}{2}\tau)A(t+\tfrac{1}{2}\tau)\cos[2ft+g(2t^2+\tfrac{1}{2}\tau^2)]dt$ (A5)

Now $P_1(\tau) = \cos(f\tau)\int A(t-\tfrac{1}{2}\tau)A(t+\tfrac{1}{2}\tau)\cos(2gt\tau)dt$ (A6)

plus the integral of a sin term which vanishes because of the symmetry of $A(t-\tfrac{1}{2}\tau)A(t+\tfrac{1}{2}\tau)$ about zero. $P_2(\tau)$ is small because of the high frequency of the modulation under the integral sign, provided $A(t)$ varies slowly as stipulated. Hence

$$P(\tau) \approx \cos(f\tau)\int A(t-\tfrac{1}{2}\tau)A(t+\tfrac{1}{2}\tau)\cos(2gt\ \tau)dt \tag{A7}$$

Similarly the quadrature match-filtered signal

$$Q(\tau) \approx -\sin(f\tau)\int A(t-\tfrac{1}{2}\tau)A(t+\tfrac{1}{2}\tau)\cos(2gt\tau)dt \tag{A8}$$

Consider the complex quadrature match-filtered signal $X(\tau) = P(\tau) + iQ(\tau)$. The envelope

$$E(\tau) = |X(\tau)| \approx \int A(t-\tfrac{1}{2}\tau)A(t+\tfrac{1}{2}\tau)\cos(2gt\tau)dt \tag{A9}$$

is a function of bandwidth, while the phase, $f\tau$, is a function only of the mid-frequency f.